

Proton quark distributions from a light-front Faddeev-Bethe-Salpeter approach

E. Ydrefors^a, T. Frederico^b

^a*Institute of Modern Physics, Chinese Academy of Sciences, Lanzhou 730000, China*

^b*Instituto Tecnológico de Aeronáutica, DCTA, 12228-900 São José dos Campos, Brazil*

Abstract

The projection onto the Light-Front of a Minkowski space Faddeev-Bethe-Salpeter equation model truncated at the valence level is applied to study the proton structure with constituent quarks. The dynamics of the model has built-in: (i) a bound diquark brought by a contact interaction, and (ii) the separation by $\sim \Lambda_{QCD}$ of the infrared and ultraviolet interaction regions. The model parameters are fine tuned to reproduce the proton Dirac electromagnetic form factor and mass. From that, the non-polarized longitudinal and transverse momentum distributions were computed. The results for the evolved non-polarized valence parton distributions suggest that: (i) the explicit consideration of the spin degree of freedom of both quark and diquark seems not relevant to it, and (ii) the comparison with the global fit from the NNPDF4.0 calls for higher Fock components of the wave function beyond the valence one.

Keywords: Faddeev-Bethe-Salpeter equation, Light-Front, proton structure, valence state, momentum distributions

Introduction. The distinctive characteristic of Quantum Chromodynamics (QCD) is its ability to dynamically enhance the interaction in the infrared (IR) region or at long distances. Phenomena like the mass generation of the light hadrons is outside the known Higgs mechanism, but it is born in the enhancement of the IR interaction among quarks and gluons, leading to chiral symmetry breaking and the quark dressing [1, 2, 3, 4]. At the same time gluons are also dressed and in extreme IR region they behave as massive particles of about 600 MeV [5] (for a recent discussion of the gluon propagator in the Landau gauge see [6]). Any successful representation of the QCD dynamics by means of models has to incorporate the strengthening of the effective interaction in IR region [7] and dressed degrees of freedom. The interaction among these dressed quarks is based on the exchange of dressed gluons, which has a range of about ~ 0.3 fm inside the hadron, where the interaction at larger distances becomes strong, or below momentum of 600 MeV $\sim 2\Lambda_{QCD}$. Therefore, to some extent the constituent quarks have a short-range interaction at low momentum, which could be parameterized effectively as a contact one, as happens in the successful phenomenology provided by Nambu-Jona-Lasinio quark models (see e.g. [8]).

The implementation of effective interactions among the constituent quarks on the hypersurface ($x^+ = t + z = 0$) within light-cone quantization [9, 10, 11, 12], allows to find the hadron state as an eigenstate of the light-front (LF) Hamiltonian. On the other hand such description leads to the partonic picture of the hadron in the ultraviolet (UV) momentum region. The hadron state expanded in the LF Fock basis defined with constituent degrees of freedom, ultimately allows to build the hadron image through the different probability densities (see e.g. [13]). The associated parton distributions to be studied in future facilities as the Electron Ion Collider (EIC) [14] and the one in China (EicC) [15], will provide precise information on the QCD nonperturbative IR physics.

Among the Fock-components of the hadron wave function, the dominant valence one can also be obtained from the projection onto the LF of the Minkowski space Bethe-Salpeter amplitude (see e.g. [16, 17]). Furthermore, the valence wave function is an eigenstate of the effective LF mass squared operator reduced to the valence sector, which can be derived from the BS equation using the quasi-potential approach applied to two bosons [18], two fermions [19] and to three-particles [20, 21]. The effective interaction contains the infinite sum over intermediate states in the Fock-space. Alternatively, the eigenvalue equation for the effective LF mass squared operator can be derived using the "it-

Email addresses: ydrefors@kth.se (E. Ydrefors), tobias@ita.br (T. Frederico)

erated resolvent method” [9].

In this work, we further study the proton within the framework of the LF projected Minkowski space Faddeev-Bethe-Salpeter (LF-FBS) equation for three particles with a contact pairwise interaction [22, 23] (see [24] for the detailed derivation within the quasi-potential approach). This valence model has been used to investigate the proton structure with the totally symmetric momentum component of the valence wave function [25] and applied recently [24] to study the proton image on the null-plane. The essential dynamical ingredient is a diquark [26], which is introduced in the model through the quark-quark amplitude, analogous to formulations of the nucleon with Euclidean continuum methods [27]. Other recent approaches to the nucleon emphasize diquark degrees of freedom (see e.g. [28, 29]).

The kernel of the LF-FBS equation applied for the proton is improved to take into account the separation between the IR and the UV interaction regions in the three-quark dynamics. This is achieved by introducing a soft cutoff of the free three-quark LF propagation in states of high virtuality. The deep unphysical ground state found previously [30] is now naturally removed. In the present formulation of the LF-FBS model the quark spin degree of freedom is not considered, as it is our goal to study the spatial non-polarized distributions of the quarks in the proton valence state, namely, the parton distribution function (PDF) and transverse momentum distribution (TMD).

LF three-quark model. We consider only the totally symmetric momentum part of the the colorless three-quark wave function corresponding to the valence nucleon state, as we are interested for the time being on the investigation of the properties associated with the momentum distributions and the image of the nucleon onto the null-plane. In this case, the valence LF wave function is written as [24]:

$$\Psi_3(\{x, \vec{k}_\perp\}) = \sum_{i=1}^3 \frac{\Gamma(x_i, k_{i\perp})}{\sqrt{x_1 x_2 x_3} (M_N^2 - M_0^2(\{x, \vec{k}_\perp\}))}, \quad (1)$$

$\{x, \vec{k}_\perp\} \equiv \{x_1, \vec{k}_{1\perp}, x_2, \vec{k}_{2\perp}, x_3, \vec{k}_{3\perp}\}$ with $\Gamma(x_i, k_{i\perp})$, where $k_{i\perp} = |\vec{k}_{i\perp}|$, being the Faddeev component of the vertex function for the bound state, $x_1 + x_2 + x_3 = 1$, $\vec{k}_{1\perp} + \vec{k}_{2\perp} + \vec{k}_{3\perp} = \vec{0}_\perp$ and $M_0^2(\{x, \vec{k}_\perp\}) = \sum_{i=1}^3 \frac{k_{i\perp}^2 + m^2}{x_i}$, is the free three-body squared mass for on-mass-shell constituents. The factorized form of the valence wave function, namely with a vertex function depending solely on the bachelor quark LF momenta, is a consequence of the effective contact interaction between the constituent

quarks, which is an idealized model resembling the successful Nambu-Jona-Lasinio model applied to model QCD [31]. It should be understood as an effective low-energy model which is meant to have significance in the IR region where constituent quarks are massive and bound forming the nucleon.

The bound state homogeneous Faddeev equation for the vertex component of the nucleon valence LF wave function, with four-point local interaction between the constituents was described in Refs. [22, 23] and applied to study the proton in [25, 24]. One physical key ingredient was missing so far in these previous studies, namely the kernel of the dynamical integral equation has to take into account the IR enhancement of the QCD interaction between the quarks [7] and the weakening at large momentum scale. However, our model four-point local interaction has its action in the UV region, while in IR quarks and gluons interact strongly according to QCD. In order to represent the physics of QCD, which undoubtedly distinguish the IR and UV dynamics, we model the kernel in a way that it is stronger at low momenta and weaker for large ones. For this aim we introduced a smooth cutoff in the integral equation for the Faddeev component of the vertex such that:

$$\Gamma(x, k_\perp) = \frac{\mathcal{F}(M_{12}^2)}{(2\pi)^3} \int_0^{1-x} \frac{dx'}{x'(1-x-x')} \times \int_0^\infty d^2 k'_\perp \frac{\Lambda(\widehat{M}_0^2)}{\widehat{M}_0^2 - M_N^2} \Gamma(x', k'_\perp), \quad (2)$$

where $\mathcal{F}(M_{12}^2)$ is the quark-quark amplitude, $\widehat{M}_0^2 = M_0^2(x, \vec{k}_\perp, x', \vec{k}'_\perp, 1-x-x', -(\vec{k}_\perp + \vec{k}'_\perp))$. Eq. (2) for $\Lambda(\widehat{M}_0^2) = 1$ was derived in detail in [24] resorting to the quasi-potential technique to perform the projection onto the LF of the three-boson BS equation in Minkowski space. Such LF equation corresponds to the truncation of the LF Fock-space only at the valence level. The form factor is introduced to cut the three-quark resolvent at large virtuality, such that

$$\frac{1}{\widehat{M}_0^2 - M_N^2} - \frac{1}{\widehat{M}_0^2 + \mu^2} = \frac{\Lambda(\widehat{M}_0^2)}{\widehat{M}_0^2 - M_N^2}, \quad (3)$$

where $\Lambda(\widehat{M}_0^2) = (M_N^2 + \mu^2)/(\widehat{M}_0^2 + \mu^2)$, which dampens the kernel when $\widehat{M}_0^2 \gg \mu^2$, without changing the low momentum region. In the IR region $F(\widehat{M}_0^2) \sim 1$, as the minimum value of the three-quark free-mass is $3m$, which is about the nucleon mass. The IR scale of the model is chosen $\mu \sim \Lambda_{QCD}$. Noteworthy that the IR enhancement of the kernel also should simulate the relevance of the coupling of the valence component to the

Model	m [MeV]	a/m	μ/m	M_{dq} [MeV]
(a)	366	2.70	1	644
(b)	362	3.60	∞	682
(c)	317	-1.84	∞	-

Table 1: Model parameters: constituent quark mass (2nd column), scattering length in units of m^{-1} (3rd column), cutoff mass in units of m (4th column) and diquark mass (5th column). The nucleon mass is 940 MeV.

higher Fock-components at large distances. In addition, the choice of the form factor eliminates the unphysical solution with $M_N^2 < 0$ appearing for the bound diquark case when $\Lambda(\widehat{M}_0^2) = 1$ [24], as we are going to show.

We observe that the quark-exchange kernel of the LF-FBS equation (2) regularized at the mass scale μ can be recognized by the appearance of the regulated free resolvent given by Eq. (3). The quark-exchange kernel is also present in the Euclidean four-dimensional three-quark BSE [4] when diquarks dominate the quark-quark interaction.

The model takes into account the quark-quark amplitude, $\mathcal{F}(M_{12}^2)$, which weights the kernel of the LF-FBS equation for the vertex function, and has the following expression in the limit of an effective contact interaction between the constituent quarks:

$$\mathcal{F}(M_{12}^2) = \frac{\Theta(-M_{12}^2)}{\frac{1}{16\pi^2 y} \log \frac{1+y}{1-y} - \frac{1}{16\pi m a}} + \frac{\Theta(M_{12}^2) \Theta(4m^2 - M_{12}^2)}{\frac{1}{8\pi^2 y'} \arctan y' - \frac{1}{16\pi m a}}, \quad (4)$$

where the $\Theta(x)$ denotes the Heaviside theta function, and its argument is the effective off-shell mass of the two-quark subsystem squared, given by

$$M_{12}^2 = (1-x)M_N^2 - \frac{k_\perp^2 + (1-x)m^2}{x},$$

$$y' = \frac{M_{12}}{\sqrt{4m^2 - M_{12}^2}}, \quad y = \frac{\sqrt{-M_{12}^2}}{\sqrt{4m^2 - M_{12}^2}}. \quad (5)$$

The scalar diquark is a pole of the quark-quark amplitude, Eq. (4), for scattering lengths $\pi/(2m) > a > 0$ associated with a diquark mass M_{dq} , which is a model parameter. The value of M_{dq} is suggested by the recent literature [26] to be around 600 MeV. In the case a is negative no physical two-body bound-state exists and the nucleon is a Borromean state. In both situations, when $\pi/(2m) > a > 0$ and $a < 0$, the quark-quark amplitude has a pole. In the former case the pole appears in the physical complex-energy sheet, while in the latter in the 2nd one, meaning the virtual state. The strong diquark correlation is manifested either for bound or

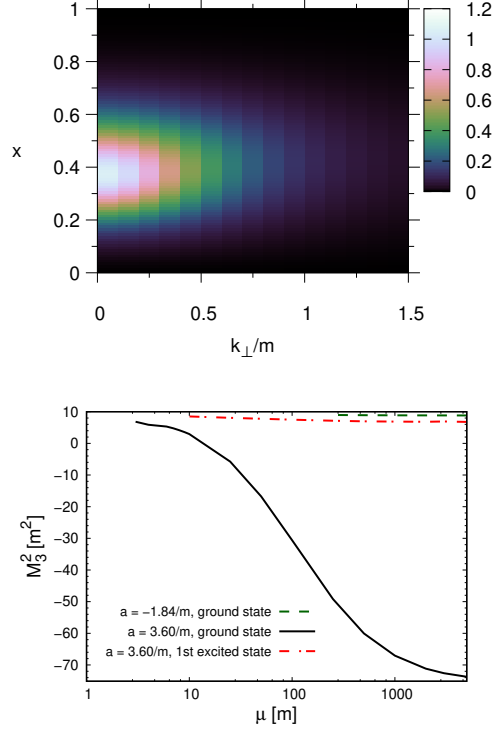


Figure 1: Upper panel: Vertex function, $\Gamma(x, k_\perp)$, in arbitrary units for model (a). Lower panel: Computed values of the squared three-body bound state mass, M_3^2 , versus the cutoff mass, μ , for $a/m = 3.60$ ground (solid line) and first excited state (dot-dashed line), and $a/m = -1.84$ (dashed line). The asymptotic limits of $\mu \rightarrow \infty$ correspond to model (b) (dot-dashed line) and to model (c) (dashed line).

virtual states and it is a consequence of the enhancement of interaction between the constituent quarks in the IR region [26]. Some choices of parameters of the model are given in Table 1, with (a) being the new one for $\mu = m$, (b) and (c) for $\mu = \infty$, which were already studied in [24]. The choice (a) of model parameters will become clear later on.

In the upper panel of Fig. 1, the Faddeev component of the vertex, $\Gamma(x, k_\perp)$, is shown. The quark mass in model (a) is chosen close to 350 MeV which is the IR value obtained in a recent LQCD calculation in the Landau gauge [32]. We note that the diquark mass of 644 MeV presents a difference of 278 MeV with respect to the quark mass, comparable to the gauge invariant result from the LQCD calculation [33] of 319(1) MeV at the physical pion mass. For the model (a) with parameters inspired by LQCD results, the three-quark system has only one bound state, which is identified with the nucleon. The vertex function is peaked at $x \sim 1/3$ and it spreads out up to $k_\perp \sim \Lambda_{QCD}$, which is about the constituent quark mass and turns even more reasonable our

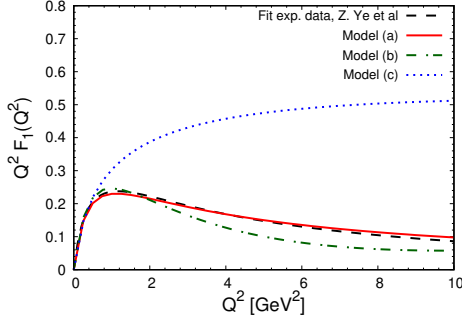


Figure 2: $F_1(Q^2)$ for model (a) (solid line), (b) (dot-dashed line) and (c) (dotted line). The empirical fit (dashed line) obtained in Ref. [34].

choice of μ . In particular, model (a) provides a fit to the Dirac form factor of the proton, as it will be shown.

To be complete, we present in the lower panel of Fig. 1, the computed values of the squared three-body mass, M_3^2 , as a function of the cutoff mass μ for the ground and first excited states for $a = 3.6/m$, and ground state in the case of $a = -1.84/m$. By decreasing the value of μ the unphysical ground state of the model with $M_3^2 < 0$ for $a = 3.6/m$ disappears and turns to a physical one. A similar effect is found for $a = 2.7/m$ which for $\mu = m$ defines the model parametrization (a) given in Table 1.

Dirac form factor. The present model accounts only for the valence state of the nucleon wave function, and it allows to obtain the Dirac form factor as discussed in detail in [24]. Resorting to the Drell-Yan condition where the plus component of the momentum transfer vanishes ($q^+ = 0$), the form factor computed with the valence component of the wave function is given by:

$$F_1(Q^2) = \int \{dx d^2k_\perp\} \Psi_3^\dagger(\{x, \vec{k}_\perp\}) \Psi_3(\{x, \vec{k}_\perp\}), \quad (6)$$

where the phase-space integral is

$$\int \{dx d^2k_\perp\} = \prod_{i=1}^2 \int \frac{d^2k_{i\perp}}{(2\pi)^2} \int_0^1 dx_i \Theta(1 - x_1 - x_2), \quad (7)$$

with $\sum_{i=1}^3 \vec{k}_{i\perp} = 0$, $\sum_{i=1}^3 x_i = 1$ and $Q^2 = \vec{q}_\perp \cdot \vec{q}_\perp$. Furthermore, choosing the Breit frame the momenta of the quarks in Eq. (6) are:

$$\begin{aligned} \vec{k}_{i\perp}^{f(i)} &= \vec{k}_{i\perp} \pm \frac{\vec{q}_\perp}{2} x_i \quad (i = 1, 2) \quad \text{and} \\ \vec{k}_{3\perp}^{f(i)} &= \pm \frac{\vec{q}_\perp}{2} (x_3 - 1) - \vec{k}_{1\perp} - \vec{k}_{2\perp}, \end{aligned} \quad (8)$$

with -(+) for f(i).

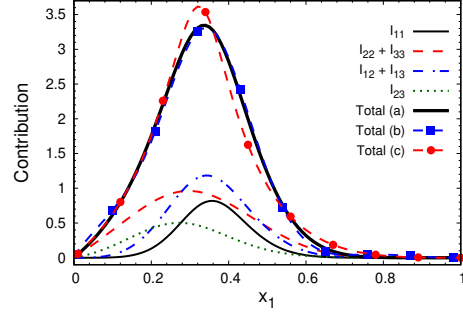


Figure 3: Valence PDF computed with model (a): I_{11} (solid thin line), $I_{22} + I_{33}$ (dashed line), $I_{12} + I_{13}$ (dot-dashed line), I_{23} (dotted line) and the total (solid thick line) normalized to 1. Results for the total PDF for model (b) (full squares) and (c) (full circles) are connected by the dashed lines.

In Fig. 2, we present the results for the proton Dirac form factor, $F_1(Q^2)$, with model (a), which was fine tuned to be consistent with the global fit to experimental data by Ye et al [34] up to 10 GeV^2 . In addition, we present the previous results [24] obtained with model (b) having a bound diquark, and with model (c) presenting a virtual diquark, both calculations have $\mu = \infty$. The IR dynamics is not privileged by models (b) and (c) and the calculated Dirac form factor is not able to reproduce the experimental fit, which is now possible. The enhancement of the interaction kernel of Eq. (2) in the IR with respect to the UV region, was achieved with the introduction of the regularization scale $\mu \sim \Lambda_{QCD}$ in Eq. (3), which finally lead the model to the experimental Dirac form factor.

Valence quark momentum distribution. The valence PDF should be given by the sum over all Fock components of the proton light-front wave function, namely:

$$\begin{aligned} f_1(x) &= \sum_{n=3}^{\infty} \left\{ \prod_i^n \int \frac{d^2k_{i\perp}}{(2\pi)^2} \int_0^1 dx_i \right\} \\ &\times \delta(x - x_1) \delta\left(1 - \sum_{i=1}^n x_i\right) \delta\left(\sum_{i=1}^n \vec{k}_{i\perp}\right) \\ &\times |\Psi_n(x_1, \vec{k}_{1\perp}, x_2, \vec{k}_{2\perp}, \dots)|^2, \end{aligned} \quad (9)$$

where n indicates the number of partons in each Fock contribution to the probability amplitude. However, in the present model, we consider only the valence component of the proton LF wave function, namely the truncation takes into account only $n = 3$, which presumably is the dominant one. It has been verified for the pion state [35] where the valence contribution accounts for 70% of the LF wave function described in terms of constituent quark degrees of freedom.

The results for the valence parton distribution (PDF) at the hadron scale are shown in Fig. 3 for model (a), (b) and (c). The PDF is obtained from the integrand of Eq. (6) for the Dirac form factor at $Q^2 = 0$ or equivalently from Eq. (9) truncated at the valence state:

$$f_1(x) = \sum_{3 \geq j \geq i \geq 1} (2 - \delta_{ij}) I_{ij}(x), \quad (10)$$

where

$$I_{ij}(x) = \int \{dx d^2k_\perp\} \frac{\delta(x - x_1)}{x_1 x_2 x_3} \frac{\Gamma(x_i, \vec{k}_{i\perp}) \Gamma(x_j, \vec{k}_{j\perp})}{(M_N^2 - M_0^2((x, \vec{k}_\perp))^2)}, \quad (11)$$

with $\sum_{i=1}^3 \vec{k}_{i\perp} = 0$ and $\sum_{i=1}^3 x_i = 1$. The contributions to the PDF indicated in the figure are identified by I_{ij} defined in Eq. (11). Due to the symmetry of the nucleon wave function under the exchange of quarks 2 and 3, it follows that $I_{22} = I_{33}$ and $I_{12} = I_{13}$, these relations are taken into account in Eq. (10). Noteworthy to find that all the contributions have about the same size, and are peaked around $1/3$, despite our choice of quark 1 to obtain the PDF. This property can be traced back to the denominator appearing in the valence wave function in Eq. (1), which is the three-quark resolvent and has its maximum value at the smallest virtuality of the three-quark system. The contribution from I_{11} corresponds to the situation where the quark 1 is picked up while the pair of quarks 2 and 3 are in a diquark correlation, which is a small fraction of the total PDF, showing that the symmetrization of the valence wave function is relevant for building the proton PDF.

All contributions to the PDF are indeed similar in magnitude, and no one is dominant, as we have already shown previously in the study of models (b) and (c) in Ref. [24]. Interesting to observe that models (a) and (b), which both present a bound diquark and provide results close to the experimental proton Dirac form factor, as seen in Fig. 2, also have very similar PDF's. This suggests that for these observables, form factor and PDF, the formation of the diquark is a dominant feature, quite independent on the cutoff mass. However, model (b) presents an unphysical ground state, which is eliminated by the introduction of the cutoff, as we have discussed.

Evolved valence PDFs. We present results for model (a) at $Q = 3.097$ GeV for the u and d valence quarks in Fig. 4. We compare with the recent results obtained with the Dyson-Schwinger Equation (DSE) approach [27]. In this work we adopted the same method as the one used in [37] for the evolution of the pion PDF. Namely, the DGLAP equation with lowest-order splitting function was used together with the effective charge from [38].

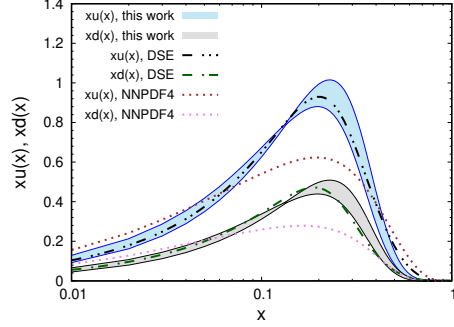


Figure 4: Valence u and d quark PDFs evolved to $Q = 3.097$ GeV. Comparison with DSE [27]. The shaded areas correspond to model (a) for $Q_0 = 0.33 \pm 0.03$ GeV. NNPDF 4.0 global fit [36] (dotted lines).

We also took into account an uncertainty with respect to the initial proton scale: $Q_0 = 0.33 \pm 0.03$ GeV [38], and compared our calculations with the results from the NNPDF 4.0 global fit¹ [36]. The model (a) produces results quite consistent with the DSE approach, which privileges the strong diquark correlation, only at large x the discrepancy becomes visible with a softer behavior from the DSE approach. The present model has a strong UV damping due to the cutoff, being not asymptotically free at large momentum, which is associated with a harder behavior at the end-point. Furthermore, it has only the contribution for the PDF from the valence light-front wave function, which is strongly peaked around $1/3$. It is expected that the higher Fock-components contribution to the PDF moves the peak towards smaller x , as the proton longitudinal momentum is shared between more than three quarks. Therefore, the value of $\langle x_q \rangle$ should be somewhat decreased, as we observe from the comparison of model (a) with NNPDF4.0 in Table 2 for the first Mellin moments.

In the present LF-FBS model the proton has 100% probability to be in the valence state, as we have considered only $n = 3$ in the Fock space decomposition of Eq. (9). We verified that the sum rule $\langle x_u \rangle + \langle x_d \rangle = 1$ is saturated at the proton initial scale by adopting the standard normalization:

$$\int_0^1 dx f_u(x) = 2 \quad \text{and} \quad \int_0^1 dx f_d(x) = 1, \quad (12)$$

where $f_q(x) = (2 - \delta_{q,d})f_1(x)$ with $f_1(x)$ normalized to 1 and obtained from Eq. (10). The assumption of

¹Shown in the Fig. 4 are the central values of the NNPDF 4.0 global fit available in the PDF database at <https://lhpdf.hepforge.org/pdfsets.html> and the data was extracted by using the LHAPDF software [39].

q	u	d
Model (a)		
$\langle x_q \rangle$	0.296 ± 0.025	0.148 ± 0.012
$\langle x_q^2 \rangle$	0.071 ± 0.009	0.036 ± 0.005
$\langle x_q^3 \rangle$	0.021 ± 0.004	0.011 ± 0.002
$\langle x_q^4 \rangle$	0.007 ± 0.002	0.004 ± 0.001
DSE [27]		
$\langle x_q \rangle$	0.303	0.137
$\langle x_q^2 \rangle$	0.077	0.032
$\langle x_q^3 \rangle$	0.032	0.009
$\langle x_q^4 \rangle$	0.010	0.003
NNPDF4.0		
$\langle x_q \rangle$	0.261	0.101
$\langle x_q^2 \rangle$	0.072	0.023
$\langle x_q^3 \rangle$	0.027	0.007
$\langle x_q^4 \rangle$	0.012	0.003

Table 2: Mellin moments, $\langle x_q^n \rangle$, of the valence quark PDF ($q = u, d$) at $Q = 3.097$ GeV for model (a) compared with the DSE [27] and the NNPDF 4.0 global fit [36], obtained by integrating the PDFs shown in Fig. 4.

only valence state in the proton at the initial scale is not fully sustained by the comparison with NNPDF4.0 global fit as shown in Table 2 at $Q = 3.097$ GeV, as the model Mellin moments $\langle x_u \rangle$ and $\langle x_d \rangle$ are clearly over estimated. On the other hand the comparison with the continuum DSE results from Ref. [27], which takes into account the detailed spin structure of the quarks and diquarks, suggests that the spin contribution is averaged out in the non-polarized PDF, as shown in both Fig. 4 and in Table 2 for the first few moments at $Q = 3.097$ GeV.

Noteworthy, the present model represents the truncation of the FBS equation at the valence level, and its full representation on the LF has to consider the contribution of an induced three-body interaction from the coupling of the valence with higher Fock-states [40, 30]. In principle, this four-dimensional FB equation model only takes into account the quark sea, and despite of that a quite relevant effect in the binding energy was found in [30]. Here, with the introduction of the soft cutoff, this effect would be somewhat reduced. However, gluons are not taken into account in this model which presumably are the main degrees of freedom to share the quark longitudinal momentum.

Transverse momentum distribution at the proton scale. The single quark transverse momentum distribution in the forward limit [41] is associated with the probability density to find a quark with momentum k_\perp

and x , when truncated to the valence component is:

$$\tilde{f}_1(k_\perp, x) = \int_0^1 dx_1 \delta(x - x_1) \int \frac{dk_{1\perp}}{(2\pi)^2} \delta(k_\perp - k_{1\perp}) \times \int_0^{2\pi} d\theta_1 \int \frac{d^2 k_{2\perp}}{(2\pi)^2} \int_0^{1-x} dx_2 |\Psi_3(\{x, \vec{k}_\perp\})|^2, \quad (13)$$

where only the dependence on $k_\perp = |\vec{k}_\perp|$ remains due to the symmetry of the wave function under rotations in the transverse plane.

The PDF is the integrated TMD on the transverse momentum:

$$f_1(x) = \int dk_\perp k_\perp \tilde{f}_1(k_\perp, x) \quad (14)$$

and the integrated TMD in the longitudinal momentum is

$$L_1(k_\perp) = k_\perp \int_0^1 dx \tilde{f}(k_\perp, x), \quad (15)$$

which represents the probability density of a single quark with transverse momentum k_\perp .

In the upper panel of Fig. 5 the valence TMD given by Eq. (13) is presented for model (a), and in the lower panel the result for the single quark transverse momentum density from Eq. (15), for models (a), (b) and (c) are shown. It is interesting to notice that the momentum scale that dominates the TMD and the integrated one is about 0.15 GeV, deep in the IR region, which is associated with the proton size in the transverse direction of ~ 1.3 fm. As seen in the lower panel of the figure, the models (a) and (b) with a bound diquark present quite similar result, and model (c) with the virtual diquark peaks at considerably lower transverse momentum, reflecting the lower binding energy (see Table 1). The TMD and the integrated one reflect and are a source of information on the IR dynamics of QCD, which in part is reflected in the binding energy of the present model.

Summary. We further develop the LF effective three-quark model for the proton, based on the notion of the dynamics dominated by the formation of diquarks. We have disregarded the momentum structure of quark-diquark vertex function, where the quark-quark amplitude is obtained from a contact interaction. The improved version of the proton model includes a soft cutoff in the kernel of the LF Faddeev equation for the vertex function [24]. This soft cutoff allows to separate the IR and UV interaction regions, with the physical effect of damping the contributions from three-quark configurations at large virtualities. This new development eliminated the unphysical ground state for bound diquarks achieved in previous calculations [30]. The present model was tuned to reproduce the Dirac proton form factor with a reasonable set of parameters: a

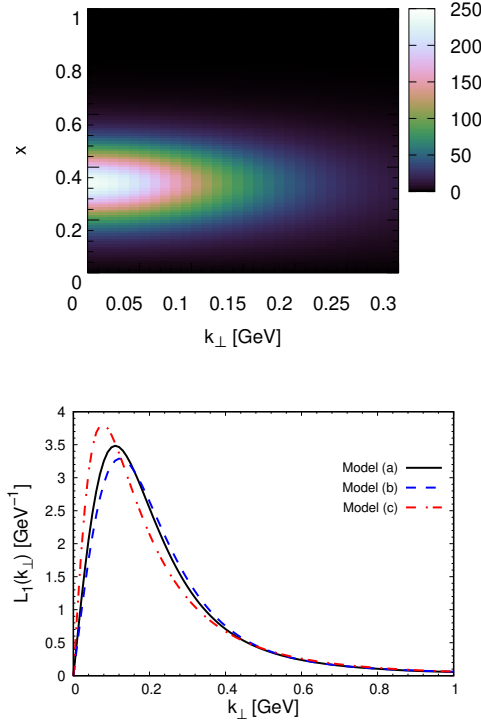


Figure 5: Transverse momentum distribution at the proton scale. Upper panel: transverse momentum distribution, $\tilde{f}_1(k_\perp, x)$ in GeV^{-2} for model (a). Lower panel: integrated transverse momentum density vs k_\perp for the (a), (b) and (c) models.

quark mass of 366 MeV, a diquark mass of 644 MeV and a cutoff of 366 MeV ($\sim \Lambda_{QCD}$), which was enough to give the proton mass. From this parameter set we explored the proton non-polarized quark longitudinal and transverse momentum distributions obtained from the valence wave function. We found that the explicit consideration of the spin degree of freedom of both quark and diquark is not relevant for the evolved non-polarized valence PDF. However, the comparison with the global fit from the NNPDF 4.0 at $Q = 3.097 \text{ GeV}$ suggests that the higher Fock-components, missed in the model wave function, could be relevant to improve the valence PDF.

Future challenges for the advance of the present nucleon effective model: the treatment Bethe-Salpeter amplitude in the four-dimensional Minkowski space [42, 43], the spin degree of freedom for polarized PDFs, and quark dressing, which will lead to further insights into the nucleon structure.

This work is a part of the project INCT-FNA #464898/2014-5. This study was financed in part by Conselho Nacional de Desenvolvimento Científico e Tecnológico (CNPq) under the grant 308486/2015-3 (TF). E.Y. thanks for the financial support of the grants

#2016/25143-7 and #2018/21758-2 from FAPESP. We thank the FAPESP Thematic grants #2017/05660-0 and #2019/07767-1.

References

- [1] A. Bashir, L. Chang, I. C. Cloët, B. El-Bennich, Y.-X. Liu, C. D. Roberts, P. C. Tandy, Collective perspective on advances in Dyson-Schwinger Equation QCD, *Commun. Theor. Phys.* 58 (2012) 79–134. [arXiv:1201.3366](#), [doi:10.1088/0253-6102/58/1/16](#).
- [2] I. C. Cloët, C. D. Roberts, Explanation and Prediction of Observables using Continuum Strong QCD, *Prog. Part. Nucl. Phys.* 77 (2014) 1–69. [arXiv:1310.2651](#), [doi:10.1016/j.pnpnp.2014.02.001](#).
- [3] T. Horn, C. D. Roberts, The pion: an enigma within the Standard Model, *J. Phys. G: Nucl. Part. Phys.* 43 (7) (2016) 073001.
- [4] G. Eichmann, H. Sanchis-Alepuz, R. Williams, R. Alkofer, C. S. Fischer, Baryons as relativistic three-quark bound states, *Prog. Part. Nucl. Phys.* 91 (2016) 1–100. [arXiv:1606.09602](#), [doi:10.1016/j.pnpnp.2016.07.001](#).
- [5] O. Oliveira, P. Bicudo, Running Gluon Mass from Landau Gauge Lattice QCD Propagator, *J. Phys. G: Nucl. Part. Phys.* 38 (2011) 045003. [arXiv:1002.4151](#), [doi:10.1088/0954-3899/38/4/045003](#).
- [6] S. W. Li, P. Lowdon, O. Oliveira, P. J. Silva, The generalised infrared structure of the gluon propagator, *Phys. Lett. B* 803 (2020) 135329.
- [7] O. Oliveira, T. Frederico, W. de Paula, The soft-gluon limit and the infrared enhancement of the quark-gluon vertex, *Eur. Phys. J. C* 80 (5) (2020) 484. [arXiv:2006.04982](#), [doi:10.1140/epjc/s10052-020-8037-0](#).
- [8] T. Hatsuda, T. Kunihiro, QCD phenomenology based on a chiral effective Lagrangian, *Phys. Rept.* 247 (1994) 221–367. [arXiv:hep-ph/9401310](#), [doi:10.1016/0370-1573\(94\)90022-1](#).
- [9] S. J. Brodsky, H.-C. Pauli, S. S. Pinsky, Quantum chromodynamics and other field theories on the light cone, *Phys. Rep.* 301 (1998) 299–486. [arXiv:hep-ph/9705477](#), [doi:10.1016/S0370-1573\(97\)00089-6](#).
- [10] J. Vary, H. Honkanen, J. Li, P. Maris, S. Brodsky, A. Harindranath, G. de Teramond, P. Sternberg, E. Ng, C. Yang, Hamiltonian light-front field theory in a basis function approach, *Phys. Rev. C* 81 (2010) 035205. [arXiv:0905.1411](#), [doi:10.1103/PhysRevC.81.035205](#).
- [11] B. Bakker, A. Bassetto, S. Brodsky, W. Broniowski, S. Dalley, T. Frederico, S. Glazek, J. Hiller, C.-R. Ji, V. Karmanov, et al., Light-Front Quantum Chromodynamics: A framework for the analysis of hadron physics, *Nucl. Phys. B Proc. Suppl.* 251 (2014) 165–174.
- [12] J. P. Vary, L. Adhikari, G. Chen, Y. Li, P. Maris, X. Zhao, Basis Light-Front Quantization: Recent Progress and Future Prospects, *Few Body Syst.* 57 (8) (2016) 695–702. [doi:10.1007/s00601-016-1117-x](#).
- [13] J. Arrington, C. A. Gayoso, P. C. Barry, V. Berdnikov, D. Binosi, L. Chang, M. Diefenthaler, M. Ding, R. Ent, T. Frederico, et al., Revealing the structure of light pseudoscalar mesons at the electron-ion collider, *J. Phys. G: Nucl. Part. Phys.* 48 (7) (2021) 075106. [doi:10.1088/1361-6471/abf5c3](#).
- [14] R. Abdul Khalek, et al., Science Requirements and Detector Concepts for the Electron-Ion Collider: EIC Yellow Report, *Nucl. Phys. A* 1026 (2022) 122447. [arXiv:2103.05419](#), [doi:10.1016/j.nuclphysa.2022.122447](#).
- [15] D. P. Anderle, et al., Electron-ion collider in China, *Front. Phys.*

- (Beijing) 16 (6) (2021) 64701. [arXiv:2102.09222](#), [doi:10.1007/s11467-021-1062-0](#).
- [16] T. Frederico, G. Salmè, Projecting the Bethe-Salpeter Equation onto the Light-Front and back: A Short Review, *Few Body Syst.* 49 (2011) 163–175. [arXiv:1011.1850](#), [doi:10.1007/s00601-010-0163-z](#).
- [17] C. Mezrag, H. Moutarde, J. Rodriguez-Quintero, From Bethe-Salpeter Wave functions to Generalised Parton Distributions, *Few Body Syst.* 57 (9) (2016) 729–772. [arXiv:1602.07722](#), [doi:10.1007/s00601-016-1119-8](#).
- [18] J. H. O. Sales, T. Frederico, B. V. Carlson, P. U. Sauer, Light front Bethe-Salpeter equation, *Phys. Rev. C* 61 (2000) 044003. [arXiv:nucl-th/9909029](#), [doi:10.1103/PhysRevC.61.044003](#).
- [19] J. H. O. Sales, T. Frederico, B. V. Carlson, P. U. Sauer, Renormalization of the ladder light front Bethe-Salpeter equation in the Yukawa model, *Phys. Rev. C* 63 (2001) 064003. [doi:10.1103/PhysRevC.63.064003](#).
- [20] J. A. O. Marinho, T. Frederico, Next-to-leading order light-front three-body dynamics, *PoS LC2008* (2008) 036. [doi:10.22323/1.061.0036](#).
- [21] K. S. F. F. Guimarães, O. Lourenço, W. de Paula, T. Frederico, A. C. dos Reis, Final state interaction in $D^+ \rightarrow K^- \pi^+ \pi^+$ with $K\pi$ I = 1/2 and 3/2 channels, *JHEP* 08 (2014) 135. [arXiv:1404.3797](#), [doi:10.1007/JHEP08\(2014\)135](#).
- [22] T. Frederico, Null-plane model of three bosons with zero-range interaction, *Phys. Lett. B* 282 (3) (1992) 409–414. [doi:https://doi.org/10.1016/0370-2693\(92\)90661-M](#).
- [23] J. Carbonell, V. A. Karmanov, Three-boson relativistic bound states with zero-range two-body interaction, *Phys. Rev. C* 67 (3) (2003) 037001. [doi:10.1103/physrevc.67.037001](#).
- [24] E. Ydrefors, T. Frederico, Proton image and momentum distributions from light-front dynamics, *Phys. Rev. D* 104 (11) (2021) 114012. [arXiv:2108.02146](#), [doi:10.1103/PhysRevD.104.114012](#).
- [25] W. R. B. de Araújo, J. P. B. C. de Melo, T. Frederico, Faddeev null-plane model of the nucleon, *Phys. Rev. C* 52 (1995) 2733–2737. [doi:10.1103/PhysRevC.52.2733](#).
- [26] M. Y. Barabanov, M. A. Bedolla, W. K. Brooks, G. D. Cates, C. Chen, Y. Chen, E. Cisbani, M. Ding, G. Eichmann, R. Ent, J. Ferretti, R. W. Gothe, T. Horn, S. Liuti, C. Mezrag, A. Pilloni, A. J. R. Puckett, C. D. Roberts, P. Rossi, G. Salmè, E. Santopinto, J. Segovia, S. N. Syritsyn, M. Takizawa, E. Tomasi-Gustafsson, P. Wein, B. B. Wojtsekhowski, Diquark correlations in hadron physics: Origin, impact and evidence, *Prog. Part. Nucl. Phys.* 116 (2021) 103835. [arXiv:2008.07630](#), [doi:10.1016/j.pnpnp.2020.103835](#).
- [27] Y. Lu, L. Chang, K. Raya, C. D. Roberts, J. Rodríguez-Quintero, Proton and pion distribution functions in counterpoint, *Phys. Lett. B* 830 (2022) 137130. [arXiv:2203.00753](#), [doi:10.1016/j.physletb.2022.137130](#).
- [28] T. J. Hobbs, M. Alberg, G. A. Miller, Euclidean bridge to the relativistic constituent quark model, *Phys. Rev. C* 95 (3) (2017) 035205. [arXiv:1608.07319](#), [doi:10.1103/PhysRevC.95.035205](#).
- [29] J. H. Alvarenga Nogueira, D. Colasante, V. Gherardi, T. Frederico, E. Pace, G. Salmè, Solving the Bethe-Salpeter Equation in Minkowski Space for a Fermion-Scalar system, *Phys. Rev. D* 100 (1) (2019) 016021. [arXiv:1907.03079](#), [doi:10.1103/PhysRevD.100.016021](#).
- [30] E. Ydrefors, J. H. Alvarenga Nogueira, V. Gigante, T. Frederico, V. A. Karmanov, Three-body bound states with zero-range interaction in the Bethe-Salpeter approach, *Phys. Lett. B* 770 (2017) 131–137. [arXiv:1703.07981](#), [doi:10.1016/j.physletb.2017.04.035](#).
- [31] S. P. Klevansky, The Nambu-Jona-Lasinio model of quantum chromodynamics, *Rev. Mod. Phys.* 64 (1992) 649–708. [doi:10.1103/RevModPhys.64.649](#).
- [32] O. Oliveira, P. J. Silva, J.-I. Skullerud, A. Sternbeck, Quark propagator with two flavors of O(a)-improved Wilson fermions, *Phys. Rev. D* 99 (9) (2019) 094506. [arXiv:1809.02541](#), [doi:10.1103/PhysRevD.99.094506](#).
- [33] A. Francis, P. de Forcrand, R. Lewis, K. Maltman, Diquark properties from full QCD lattice simulations (6 2021). [arXiv:2106.09080](#).
- [34] Z. Ye, J. Arrington, R. J. Hill, G. Lee, Proton and Neutron Electromagnetic Form Factors and Uncertainties, *Phys. Lett. B* 777 (2018) 8–15. [arXiv:1707.09063](#), [doi:10.1016/j.physletb.2017.11.023](#).
- [35] W. de Paula, E. Ydrefors, J. H. Alvarenga Nogueira, T. Frederico, G. Salmè, Observing the Minkowskian dynamics of the pion on the null-plane, *Phys. Rev. D* 103 (1) (2021) 014002. [arXiv:2012.04973](#), [doi:10.1103/PhysRevD.103.014002](#).
- [36] R. D. Ball, et al., The path to proton structure at 1% accuracy, *Eur. Phys. J. C* 82 (5) (2022) 428. [arXiv:2109.02653](#), [doi:10.1140/epjc/s10052-022-10328-7](#).
- [37] W. de Paula, Y. E., J. H. Alvarenga Nogueira, T. Frederico, G. Salmè, Parton distribution function in a pion with Minkowskian dynamics, *Phys. Rev. D* 105 (2022) L071505. [arXiv:2203.07106](#), [doi:10.1103/PhysRevD.105.L071505](#).
- [38] Z. F. Cui, M. Ding, J. M. Morgado, K. Raya, D. Binosi, J. Rodríguez-Quintero, S. M. Schmidt, *Eur. Phys. J. A* 58 (2022) 10.
- [39] A. Buckley, J. Ferrando, S. Lloyd, K. Nordstrom, B. Page, M. Ruefenacht, M. Schoenherr, G. Watt, Lhapdf6: parton density access in the LHC precision era, *Eur. Phys. J. C* 75 132. [arXiv:1412.7420](#), [doi:10.1140/epjc/s10052-015-3318-8](#).
- [40] V. A. Karmanov, P. Maris, Manifestation of three-body forces in three-body Bethe-Salpeter and light-front equations, *Few Body Syst.* 46 (2009) 95–113. [arXiv:0811.1100](#), [doi:10.1007/s00601-009-0054-3](#).
- [41] C. Lorcé, B. Pasquini, M. Vanderhaeghen, Unified framework for generalized and transverse-momentum dependent parton distributions within a 3Q light-cone picture of the nucleon, *JHEP* 05 (5) (2011) 041. [doi:10.1007/jhep05\(2011\)041](#).
- [42] E. Ydrefors, J. H. Alvarenga Nogueira, V. A. Karmanov, T. Frederico, Solving the three-body bound-state Bethe-Salpeter equation in Minkowski space, *Phys. Lett. B* 791 (2019) 276–280. [arXiv:1903.01741](#), [doi:10.1016/j.physletb.2019.02.046](#).
- [43] E. Ydrefors, J. H. Alvarenga Nogueira, V. A. Karmanov, T. Frederico, Three-boson bound states in Minkowski space with contact interactions, *Phys. Rev. D* 101 (9) (2020) 096018. [arXiv:2005.07943](#), [doi:10.1103/PhysRevD.101.096018](#).